A 1.94 to 2.55 GHz, 3.6 to 4.77 GHz Tunable CMOS VCO Based on Double-Tuned, Double-Driven Coupled Resonators

Burak Çatlı, *Student Member, IEEE*, and Mona Mostafa Hella, *Member, IEEE*

***Abstract*—This paper presents a multi-band CMOS VCO using a double-tuned, current-driven transformer load. The dual frequency range oscillator is based on enabling/disabling the driving current in the secondary port of the transformer. This approach eliminates the effect of switches connected directly to the VCO tank whose capacitance and on-resistance affect both the tuning range and the phase noise of a typical multi-band oscillator. The relation between the coupling coefficient of the transformer load, selection of frequency bands, and the resulting quality factor at each band is investigated. The concept is validated through measurement results from a prototype fabricated in 0.25 μm CMOS technology. The VCO has a measured tuning range of 1.94 to 2.55 GHz for the low frequency range and 3.6 to 4.77 GHz for the high frequency range. It draws a current of 1 mA from 1.8 V supply with a measured phase noise of −116 dBc/Hz at 1 MHz offset from a 2.55 GHz carrier. For the high frequency band, the VCO draws 10.1 mA from the same supply with a phase noise of −122.8 dBc/Hz at 1 MHz offset from a 4.77 GHz carrier.**

***Index Terms*—CMOS voltage controlled oscillators, coupled resonators, multi-band VCO, software defined radio, transformer-based oscillators.**

I. Introduction

THE wireless scenario for mobile and portable communications is rapidly changing from single standard systems to multi-mode terminals, with attention geared towards software defined radios and cognitive radios. Cognitive radio (CR) has recently emerged as an umbrella term for systems that can adapt to changing conditions so as to dynamically use the spectrum in an opportunistic manner. The adaptation/reconfigurability functions will be handled by adaptive frequency-agile RF transceivers which are viewed as the foundation of CR in its most extreme form of a radio that can jump in and out of any band and any operating mode. The frequency synthesizer for such a radio has to provide all necessary LO frequencies within the widely used spectrum from 600 MHz to 6 GHz with proper channel spacing. In addition, all performance requirements, phase noise being the most challenging, must be fulfilled.

Manuscript received November 07, 2008; revised April 19, 2009. Current version published August 26, 2009.

The authors are with the Electrical, Computer, and Systems Engineering Department, Rensselaer Polytechnic Institute, Troy, NY 12180 USA (e-mail: hellam@ecse.rpi.edu; catlib@rpi.edu).

Color versions of one or more of the figures in this paper are available online at http://ieeexplore.ieee.org.

Digital Object Identifier 10.1109/JSSC.2009.2023155

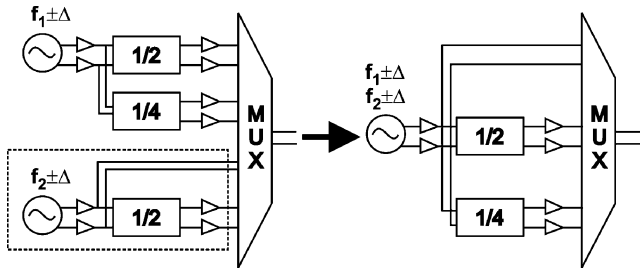

Fig. 1. (a) Typical multi-band frequency generation architecture. (b) Reduction in number of components by replacing multiple oscillators with a single dual-band oscillator.

A number of local-oscillator (LO) frequencies are typically needed to cover such a wide spectrum. Since oscillators consume a substantial part of the chip area and battery power, methods to generate multiple LO frequencies in a compact design can be very effective for power and area savings. In many radio architectures, particularly in multi-mode and multi-band systems, the required local-oscillator frequencies are not necessarily harmonically related. Thus, the main focus of the research so far has been on offering multi-band frequency generators based on local oscillators with additional processing through frequency division, frequency up-/down-conversion, and multiplexing functions [1]–[5] [Fig. 1(a)]. The tuning range of each individual local oscillator determines their total number and the required additional frequency processing circuitry. Published research has either focused on wideband but single range oscillators [6]–[10], or multi-band but limited tuning range in each band [11]–[14]. Magnetic tuning or transformer based tuning [15] has also recently received much interest as an alternative technique to overcome the limited tuning capability of varactors in scaled CMOS processes, with emphasis on continuous tuning over a wide frequency range by changing the primary to secondary current ratio. Other examples of multi-band/wide-band oscillators are reported in [16]–[20].

This paper details the concept of coupled driven resonators and applies it to the design of a CMOS VCO that is capable of operating in two widely separated bands, while simultaneously achieving wide tuning range in each band. The relation between the coupling coefficient of the transformer load, selection of frequency bands, and the resulting quality factor at each band is investigated. This approach would allow hardware sharing of the divider and mixing functions [Fig. 1(b)] that would ultimately decrease the power and area consumptions relative to traditional

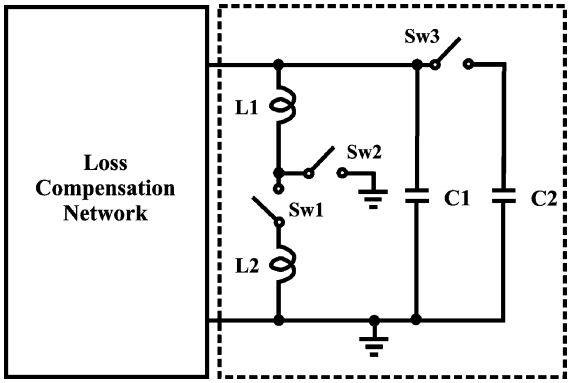

Fig. 2. Switched inductor/capacitor tank for multi-band operation.

techniques. It can also provide lower current consumption compared to continuous magnetic tuning of transformer loads by utilizing varactor tuning within each band and injecting current in the secondary winding only when switching from one frequency range to the other.

The paper is organized as follows. Section II discusses the advantages of coupled resonators versus switched resonators. Section III details the analysis of double-driven double-tuned transformer as a multi-band resonator. The design of the VCO is covered in Section IV, while measurement results are presented in Section V. Finally, conclusions are given in Section VI.

II. Switched Versus Coupled Resonators

A. Switched Inductors and Capacitors

Multi-band LC oscillators have been traditionally realized by changing the effective inductance and capacitance of the VCO tank through adding and/or subtracting L and C elements using MOS switches [11]–[14]. The basic concept is illustrated in Fig. 2. The effective inductance and capacitance of the tank are created with the combination of inductors L1, L2 and C1, C2. If switch sw2 is closed and the sw1 and sw3 are open, the oscillator generates a signal at frequency

$$\omega_1 = \frac{1}{\sqrt{L_1 C_1}}. \tag{1}$$

However, if sw1 and sw3 are closed and sw2 is opened, the oscillation frequency becomes

$$\omega_2 = \frac{1}{\sqrt{(L_1 + L_2)(C_1 + C_2)}}. \tag{2}$$

Other combinations of switches lead to different resonance frequencies. There are two factors that limit the overall performance of this approach. The first limitation originates from the nature of any real switch. The switches used in the reconfigurable tank introduce substantial parasitic resistance and capacitance, which affects the quality factor of the tank and the tuning range. The inductors connected in series in the multi-band resonator are redrawn in Fig. 3 to illustrate the effect of the switch parasitics. In Fig. 3, parasitic resistances RL1 and RL2, which determine the quality factor of the inductors, represent the loss of L1 and L2, respectively, while the switch symbol is replaced by a MOS transistor. When the switch is closed (the MOS

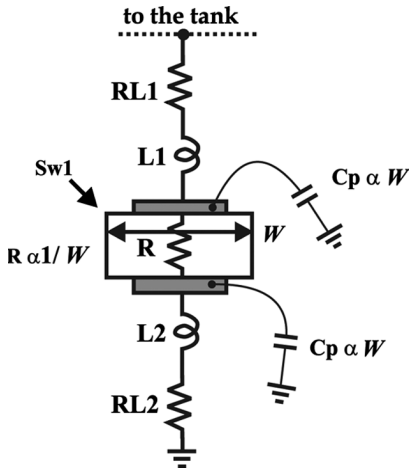

Fig. 3. Switched inductor and parasitic elements of the MOS switch.

transistor is turned on), the channel resistance of the switch is added to total tank parasitic resistance. Because this additional resistance degrades the tank Q and accordingly the VCO's phase noise, it is desired to minimize the channel resistance. In some cases, the control voltage that turns on the MOS transistor can be set to a value higher than the nominal voltage given by the technology. Under nominal supply voltage, the only way to reduce the switch resistance is to increase the transistors size (in some examples, ranging from $960\ \mu\text{m}/0.18\ \mu\text{m}$ to $2000\ \mu\text{m}/0.18\ \mu\text{m}$ [11], [12]), which also increases the parasitic capacitance of the switch, thereby reducing the tuning range of the VCO. It is clear from the above discussion that there is a trade-off between tuning range and phase noise in the switch design. Fig. 4 shows the simulated small signal capacitance and channel resistance in $0.25\ \mu$m and $0.18\ \mu$m CMOS technologies for an nMOS switch transistor as a function of channel width and bias voltage. In the simulations, the gate of the MOS transistor is connected to VDD (2.5 V and 1.8 V) and the drain and the source of the transistor are shorted and connected to a common-mode voltage VCM (0.9 V and 1.25 V) and VCM/2 (0.45 V and 0.625 V). For the nMOS switch in $0.25\ \mu$m, the simulations show that as the channel width increases, channel resistance is reduced but still remains one of the major contributors to the tank loss. These simulations also show that the switch channel resistance is very sensitive to the common-mode voltage and for best performance the common-mode voltage should be kept as low as possible. This may limit the oscillator topology, leaving pMOS transistors as the only alternative for the negative resistance circuit and/or may put some limitation on the output buffer design because of very low common-mode level of the generated signal. Finally, for a reasonable aspect ratio, the switch exhibits a high parasitic capacitance (1–3 pF) as shown in Fig. 4(a). This parasitic capacitance would ultimately limit the tuning range.

To consider the effect of technology scaling, the MOS switch is also simulated in a $0.18\ \mu$m CMOS technology. Although the channel resistance remains relatively constant with respect to the former case, the contribution of the parasitic capacitance of the nMOS switch drops. However, even for a $0.18\ \mu$m CMOS technology, the switch still introduces a high parasitic capacitance to the tank. The performance limitation that comes from

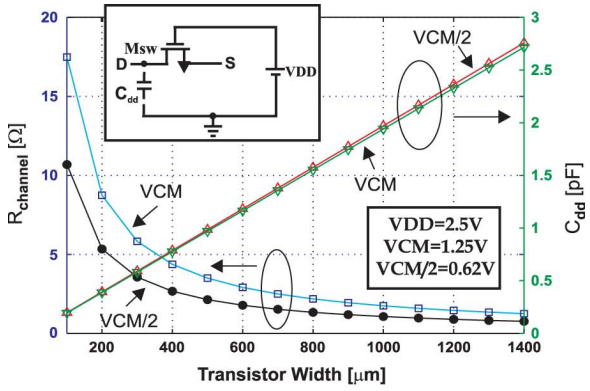

(a)

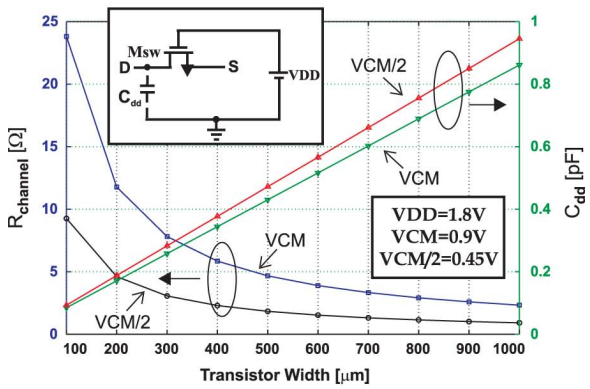

(b)

Fig. 4. The MOS switches' parasitic resistance and capacitance as a function of size and bias in (a) a 0.25 μm and (b) a 0.18 μm CMOS technology.

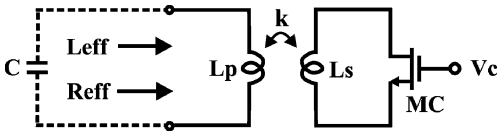

Fig. 5. Resistively tuned coupled resonators.

the parasitic capacitance of the MOS switch may be exemplified better if we consider a case study such as a 2.4 GHz oscillator. If we select the tank inductance as 2.7 nH, the remaining total capacitance budget is around 1.6 pF. Thus, the 1 pF parasitic capacitance that originates from the nMOS switch would severely limit the tuning range leaving less than 50% of the capacitance budget for the varactors. In [14], it is reported that the quality factor of a switched resonator is 30% less than that of a stand-alone inductor. From the Leeson equation, this would translate to a 3 dB difference in phase noise performance.

B. Resistively Tuned-Coupled Resonators

A variation of the switched inductor technique is realized as a variable inductor. The variable inductor is created in a coupled inductor form as shown in Fig. 5. The MOS transistor connected in parallel to the secondary winding is used as a variable resistor. The channel resistance of the MOS transistor can be adjusted by changing its gate voltage, which changes the effective inductance Leff and resistance Reff seen at the primary port. Thus, the LC product of the tank is varied for tuning purposes.

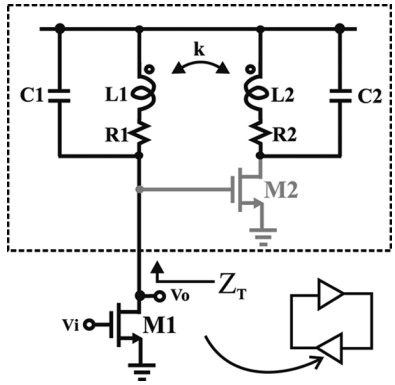

Fig. 6. Double-tuned transformer connected to a gain stage (M1).

The technique discussed above has been employed in a number of published oscillators [21]–[24]. In some applications, the control voltage Vc is changed continuously while in others, it is just used to turn on/off the device. Regardless of the used control method, the technique is based on a loss mechanism. When the switch transistor MC is off, it exhibits high impedance leaving the parasitic elements of Ls as the only loss in the secondary winding. However, when the transistor is turned on gradually, the finite channel resistance of the transistor starts to contribute to the secondary winding loss. The loss in the secondary winding is transferred from secondary to primary winding via magnetic coupling. Thus, this technique reduces the quality factor of the inductor, increasing its resistive loss and degrading the phase noise performance.

III. Driven, Double-Tuned Transformer as a Dual-Band Resonator

In many design cases, magnetic coupling can provide a unique way to improve the circuit performance. Single-tuned transformers and double-tuned transformers have already been used as impedance matching circuits and loads [25], [26]. In this section, the oscillation conditions for the single-driven and double-driven transformers are derived to illustrate the band switching mechanism. In addition, the relation between transformer coupling coefficient, tank quality factor at the two bands, and the VCO performance parameters are discussed.

A. Double-Tuned Single-Driven Transformer

For a multi-band VCO, multiple resonance points in the impedance characteristic of the load over frequency is required. For dual resonance point, the load can be realized with a transformer where capacitors are placed in parallel to the primary and secondary windings. This is known as double-tuned transformer [27], [28]. If the double-tuned transformer is connected to a driver transistor as shown in Fig. 6, we refer to this as a double-tuned, single-driven transformer. In the following analysis, transistors M2 is OFF, and its effect is ignored. In Fig. 6, the gain stage, formed by the driver transistor M1 is loaded by the double-tuned transformer which has four energy storage elements, thus two resonance points in the frequency spectrum. L_1 and L_2 are the inductances of primary and secondary ports, R_1, R_2 are loss elements of the tank and C_1, C_2 are the total capacitances of each tank, including the varactor

and other parasitic capacitances, while k is the coupling coefficient between the windings. The transfer function of the gain stage, Vo(s)/Vi(s), has gains around the resonance frequencies ω_1 and ω_2 that are the product of the transconductance and the tank impedances at these frequencies. The input impedance of double-tuned tank can be derived as in (3), shown at the bottom of the page. The resonance frequencies of the network are given by

$$\omega_{1,2} = \sqrt{\frac{2}{L_1C_1 + L_2C_2 \pm \sqrt{(L_1C_1 - L_2C_2)^2 + 4k^2L_1C_1L_2C_2}}}. \tag{4}$$

To get more insight into the oscillation mechanism, the special case of a balanced double-tuned network ($L_1 = L_2 = L, C_1 = C_2 = C$ and $R_1 = R_2 = R$) is considered. We can rewrite the resonance frequencies for the balanced case as

$$\omega_{1,2} = \frac{1}{\sqrt{LC(1 \pm k)}} = \frac{\omega_O}{\sqrt{1 \pm k}}. \tag{5}$$

The magnitude and phase of the input impedance of the balanced double-tuned network is shown in Fig. 7 where

$$z_1 = |Z_T(j\omega)|\Big|_{\omega=\omega_1} \approx \frac{Q(1+k)}{2}\sqrt{\frac{(1+k)L}{C}} \tag{6}$$

and

$$z_2 = |Z_T(j\omega)|\Big|_{\omega=\omega_2} \approx \frac{Q(1-k)}{2}\sqrt{\frac{(1-k)L}{C}} \tag{7}$$

where $Q = \omega L/R$ is the quality factor of the stand-alone inductors in the transformer.

To examine the conditions required for oscillation when using the double-tuned network as the oscillator tank, the Barkhausen's oscillation criteria are used:

$$\angle T(j\omega_O) = n\,x\,360^\circ \quad \text{and} \quad |T(j\omega_O)| > 1 \tag{8}$$

where $T(j\omega)$ is the loop transfer function, ω_o is the frequency at which the frequency shift around the loop is zero. Due to the symmetry of the gain stages of the cross-coupled topology, the transfer function of a single stage can be considered as the loop gain expression to study the oscillation condition. Thus, we have

$$|T(j\omega)| = gm_1\,|Z_T(j\omega)|\,. \tag{9}$$

From Fig. 7(c), it is clear that the phase condition is met at both ω_1 and ω_2. For the gain condition, it can be assumed that gm_1 is fairly equal at both frequencies. Although the gain and phase conditions can be satisfied at both frequencies, the oscillation

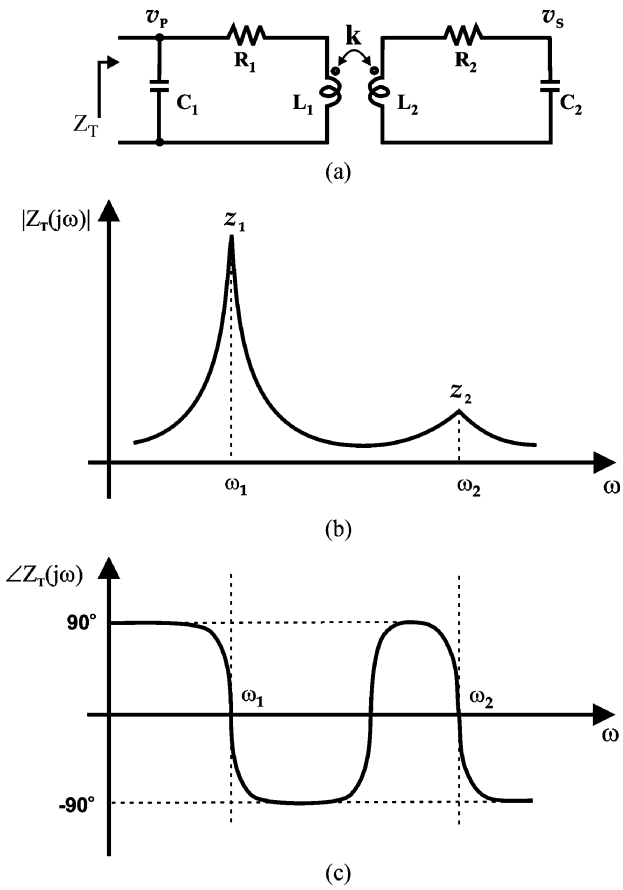

Fig. 7. The magnitude and phase of the impedance characteristic of a double-tuned transformer.

starts at one of the resonance frequencies and fails at the other. The underlying difference originates from the parallel equivalent loss resistances, z_1 and z_2. From (6) and (7)

$$z_1 \approx z_2\left(\frac{1+k}{1-k}\right)^{3/2}. \tag{10}$$

Thus, as gm_1 increases to start the oscillation, the following condition is satisfied first.

$$|T(j\omega)|\,|_{\omega=\omega_1} = gm_1z_1 \approx gm_1\left(\frac{Q(1+k)}{2}\sqrt{\frac{(1+k)L}{C}}\right) > 1 \tag{11}$$

and the circuit starts to oscillate at ω_1. If gm_1 increases further, the loop gain at ω_2 can achieve a value higher than 1, compensating the low magnitude of z_2 with respect to z_1. This may lead to a concurrent oscillation at ω_1 and ω_2. Although a stable concurrent oscillation mechanism is a more complex phenomenon

$$Z_T(s) = \frac{(1-k^2)L_1L_2C_2s^3 + (L_2R_1 + L_1R_2)C_2s^2 + (L_1 + R_1R_2C_2)s + R_1}{(1-k^2)L_1L_2C_1C_2s^4 + (L_2R_1 + L_1R_2)C_1C_2s^3 + (L_1C_1 + L_2C_2 + R_1R_2C_1C_2)s^2 + (R_1C_1 + R_2C_2)s + 1} \tag{3}$$

[30], we can roughly state that the following condition should be satisfied to avoid the possibility of concurrent oscillations:

$$|T(j\omega)|\ |_{\omega=\omega_2} = gm_1 z_2 \approx gm_1 \left(\frac{Q(1-k)}{2} \sqrt{\frac{(1-k)L}{C}} \right) < 1. \quad (12)$$

B. Double-Tuned, Double-Driven Transformer

Section III-A emphasized the importance of having a magnitude difference between parallel equivalent loss resistances at ω_1 and ω_2 to create an oscillation at only one band. However, for a single-driven double-tuned transformer network, gm_1 is the only control parameter that can start oscillation at one band or may trigger concurrent oscillations but cannot provide band switching. To enable band switching, the resonator characteristic needs to be reconfigured to modify the loop gain equations at both bands. Consider Fig. 6 again, while including the effect of the second driver transistor M2 (shown in gray) which drives the secondary port of the double-tuned transformer. In the modified configuration, the main gain transistor is still M1, and all the circuit elements in dashed box are treated as a resonator including M2. The equivalent circuit of double-driven resonator is given in Fig. 8. Transistor M2 is modeled as a transconductance stage whose current is controlled by primary port voltage v_P. The input impedance of the double-driven configuration Z_{T-DD} can be derived as shown in (13) at the bottom of the page. The introduction of gm_2 may cause changes in the amplitude ratios of secondary to primary inductor currents (i_{L2}/i_{L1}) as well as phase differences between these currents for the double-driven case with respect to the single-driven case. This can affect the contribution of the mutual inductance M, varying the resonance frequencies. This is evident from (13) where gm_2 appears in the denominator of the impedance of the double-driven configuration Z_{T-DD}. To guarantee that the location of resonance frequencies is fixed regardless of the addition of transistor M2, we will examine the effect of g_{m2} on the inductor currents ratios and the phase difference between these currents compared to the single-driven, double-tuned transformer case. The inductor current ratios for the double-driven compared to single-driven double-tuned

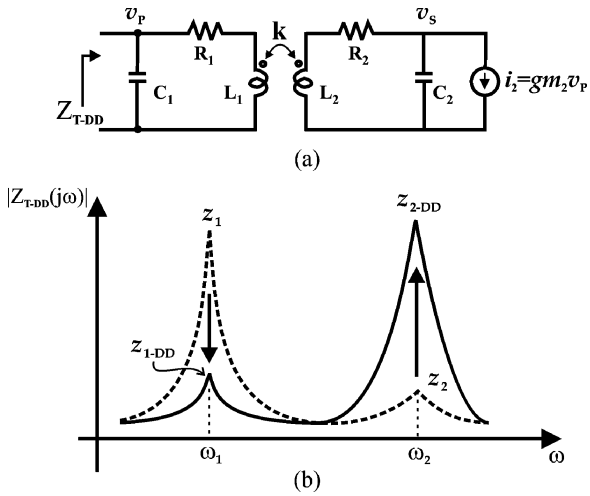

Fig. 8. Tank impedance of double-tuned, double-driven transformer. The secondary of the transformer is driven by a transconductance stage gm_2.

transformer is given as in (13), where i_{L1} and i_{L2} are the currents in the primary and secondary inductors, respectively. Examining (14), also at the bottom of the page, shows that the magnitude of the ratio is fairly constant over the frequency range and is approximately equals to 1. Similar analysis for the phase difference of the currents reveals a consistent behavior. Thus, the resonance frequencies given in (4) and (5) are still valid for the double-driven case.

The parallel equivalent loss resistances at the resonance frequencies can be derived for the double-tuned, double-driven balanced transformer as in (15) and (16), shown at the bottom of the next page. Equations (15) and (16) show the effect of gm_2 on the resonator characteristic. As gm_2 increases, the denominator of z_{2-DD} decreases while that of z_{1-DD} increases. This reduces the loop gain at ω_1, suppressing its resonance point and failing the oscillation, while increasing the loop gain at ω_2 boosting its resonance point and enabling the oscillation. Oscillation at ω_2 starts when the loop gain satisfies the condition shown in (17) at the bottom of the next page. Similar to the former case, the low-band loop gain must be kept below 1 to avoid any concurrent oscillation [see (18) at the bottom of the next page]. This discussion shows that by turning on and off the transconductance stage M2, the resonator switches between single-driven

$$Z_{T-DD}(s) = \frac{(1-k^2)L_1L_2C_2s^3+(L_2R_1+L_1R_2)C_2s^2+(L_1+R_1R_2C_2)s+R_1}{(1-k^2)L_1L_2C_1C_2s^4+(L_2R_1+L_1R_2)C_1C_2s^3+(L_1C_1+L_2C_2+R_1R_2C_1C_2)s^2+(R_1C_1+R_2C_2+gm_2k\sqrt{L_1L_2})s+1} \quad (13)$$

$$\left| \frac{\frac{i_{L2-DD}(s)}{i_{L1-DD}(s)}}{\frac{i_{L2}(s)}{i_{L1}(s)}} \right|_{s=j\omega} = \left| \frac{k\sqrt{L_1L_2}L_2C_2^2s^3 + gm_2L_1L_2C_2s^2 + k\sqrt{L_1L_2}C_2s + gm_2L_1)}{k\sqrt{L_1L_2}L_2C_2^2s^3 + gm_2k^2L_1L_2C_2s^2 + k\sqrt{L_1L_2}C_2s} \right|_{s=j\omega} \quad (14)$$

and double-driven modes, maintaining the location of the resonance frequencies but reshaping the magnitude of their respective input impedances, which enables the band-switching mechanism.

While the previous analysis of the oscillation conditions is given for the balanced double-tuned transformer for mathematical brevity, the unbalanced transformer is more practical in actual implementations for the following reasons. In the balanced topology, once the LC product is selected, the only design parameter that can be varied is the coupling coefficient, k. However, for a given LC product, design parameter k may not be enough to cover specific frequency bands. In the case of unbalanced transformer, the LC products for primary and secondary port can be selected independently. Thus, the unbalanced transformer would provide three independent design parameters that lead to better flexibility in covering any two bands.

The main distinctions between the proposed technique and former techniques discussed in Section II are summarized as follows.

1) The proposed technique uses current sources for band switching. Thus, the band switching mechanism is based on the driving currents and their relative phases with respect to each other. This is an advantage over the switched inductor/capacitor techniques that places the switch in the signal generation loop and degrades the phase noise stability as discussed in Section II.
2) The proposed technique provides area savings compared to uncoupled resonators. The magnetic coupling, which is avoided in previous techniques [12], is intentionally created in the proposed resonator interleaving the primary and the secondary inductors. Thus, there is no need for special orthogonal placement of the individual tank inductors.
3) In Fig. 5, Reff, the effective parallel loss resistance of the tank, is a strong function of tank swing due to the nature of the MOS transistor operating in the triode region. Thus, it causes strong nonlinearity that leads to AM/PM conversion, degrading phase noise performance. In the proposed technique, due to the relatively high output impedance of the current sources, band-switching mechanism does not cause any AM/PM conversion or other nonlinearities that may degrade spectral purity.

C. Effect of Coupling Coefficient on the VCO Performance Parameters

Fig. 9 shows the interaction between coupling coefficient k, location of resonance frequencies, quality factor of resonance points and power consumption. For all cases, an arbitrary unbalanced double-tuned transformer network is considered, the electrical parameters of primary and secondary tank elements are kept constant and only k and gm_2 are changed where applicable.

In Fig. 9(a), a single-driven, double-tuned transformer is considered. As the coupling coefficient varies from 0.4 to 0.7, the resonance frequencies, parallel equivalent loss resistances at these frequencies and quality factors vary. As the coupling coefficient increases, the quality factor and the parallel loss resistance increase at the first resonance frequency, while they degrade at the second resonance frequency. Since the single-driven case is applicable for low-band operation, selecting a high coupling coefficient may seem a good design approach. However, the coupling factor selection should be made considering its effects on high-band performance as illustrated in Fig. 9(b). In Fig. 9(b), the tank characteristics are plotted for the double-driven resonator for a fixed gm_2.

$$z_{1\_DD} = \left|Z_{T\_DD}(j\omega)\right|\,|_{\omega=\omega_1} \approx \frac{1}{\sqrt{gm_2^2 + \frac{4C}{(1+k)^{3/2}Q}\left(\frac{1}{(1+k)^{3/2}QL} + gm_2\omega_O\right)}} \tag{15}$$

$$z_{2\_DD} = |Z_{T-DD}(j\omega)|\,|_{\omega=\omega_2} \approx \frac{1}{\sqrt{gm_2^2 + \frac{4C}{(1-k)^{3/2}Q}\left(\frac{1}{(1-k)^{3/2}QL} - gm_2\omega_O\right)}} \tag{16}$$

$$|T_R(j\omega)|\;|_{\omega=\omega_2} = gm_1 z_2 \approx gm_1 \left(\frac{1}{\sqrt{gm_2^2 + \frac{4C}{(1-k)^{3/2}Q}\left(\frac{1}{(1-k)^{3/2}QL} - gm_2\omega_O\right)}}\right) > 1 \tag{17}$$

$$|T_R(j\omega)|\;|_{\omega=\omega_1} = gm_1 z_1 \approx gm_1 \left(\frac{1}{\sqrt{gm_2^2 + \frac{4C}{(1+k)^{3/2}Q}\left(\frac{1}{(1+k)^{3/2}QL} + gm_2\omega_O\right)}}\right) < 1 \tag{18}$$

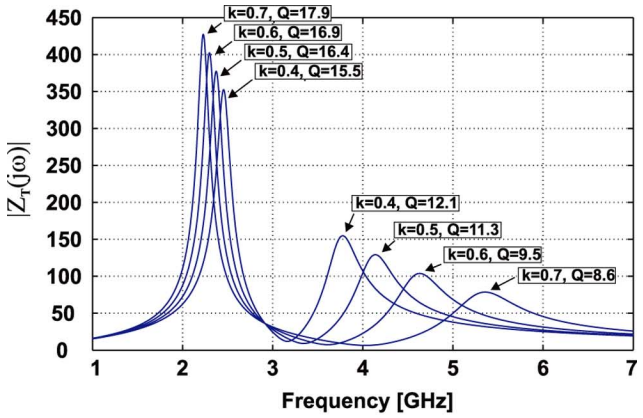

(a)

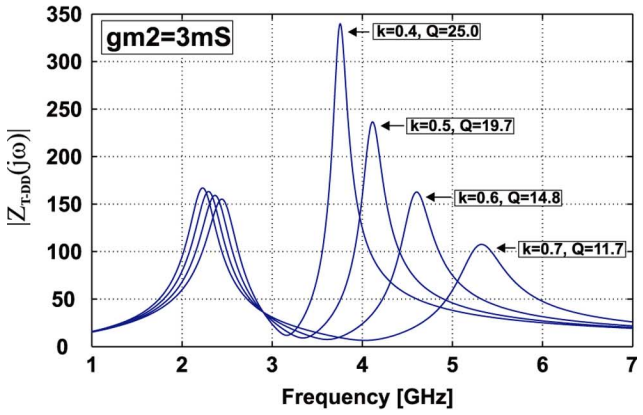

(b)

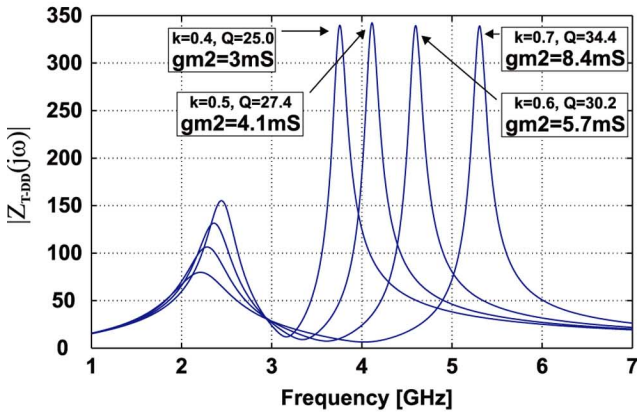

(c)

Fig. 9. The effect of coupling coefficient k and transconductance of the secondary driver stage gm_2 on the impedance characteristic of double-tuned transformer tank, (a) Single-driven transformer, (b) Double-driven transformer with fixed gm_2, and (c) Double-driven transformer with variable gm_2 to equalize the effective negative resistance at the second resonance point.

Interestingly, while $k = 0.7$ gives the highest quality factor and parallel loss resistance at low-band ($Q = 17.9$), it leads to the lowest quality factor at high-band ($Q = 11.7$). On the other hand, $k = 0.5$ provides comparable performance at low-band ($Q = 16.4$) and high-band ($Q = 19.7$). Although the numbers and optimum k may vary for different specifications, as a guideline, a moderate k value around $0.4 \sim 0.5$ would provide a balanced performance at both bands. This discussion

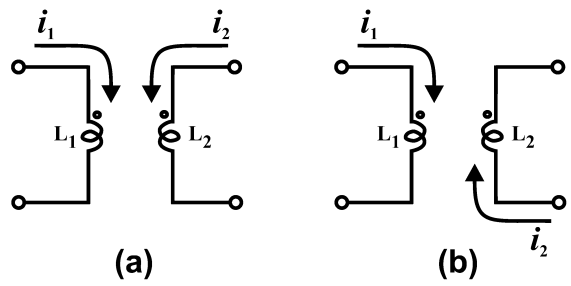

Fig. 10. Relative directions of ac currents in low-band and high-band operation.

may trigger the question: Would $k = 0$ or $k = 0.1$ provide a better performance VCO? In fact, these values are so low that they can be considered parasitic coupling coefficients between two stand-alone inductors that are located in an orthogonal orientation [12]. As k decreases, any transformer topology would suffer from considerable increase in area, approaching that of two stand-alone inductors.

The last scenario shown in Fig. 9(c) shows the relation between coupling coefficient and power consumption. To compensate for the drop in parallel loss resistance that may stop oscillations at higher coupling coefficients, additional currents can be injected into the secondary of the transformer (increasing gm_2). Fig. 9(c) shows the required gm_2 in each case to equalize equivalent loss resistance at different coupling coefficients. From Fig. 9(c), $k = 0.7$ requires 2.8 times higher gm_2 to reach the same parallel loss resistance as $k = 0.4$, which may translate to several times higher current consumption for the same size of transistor M2. Thus, the high coupling coefficient translates to higher power consumption to meet the loop gain condition at the high-band. In summary, the optimization of the double-tuned unbalanced transformer network for a dual-band VCO application is a multi-dimensional process. It involves the selection of the location of band centers, tuning range in each band, phase noise requirements over the bands, as well as area and power consumption limits.

D. Quality Factor of the Tank at Low-Band and High-Band

The transformer as a resonator in single-band oscillators has been the subject of previous publications [26]. In most of these applications, the transformer has been used for quality factor enhancement. However, recent publications [29], [30] have shown that there are misconceptions about transformer based resonator design, and whether it actually improves the phase noise of the oscillator versus traditional LC oscillator design. While it is true that for any quality factor improvement, the currents in the windings should be in phase as shown in Fig. 10(a), given the same area as the transformer, a stand-alone inductor may provide better values for the quality factor [31].

For low-band operation, the AC current in the primary winding i_p and the induced current in the secondary winding i_s are in phase. Thus, an improved quality factor with respect to that of the stand-alone primary inductor is expected. However, this improvement should be evaluated in the frame of the previous discussion. For the high-band operation, as shown in Fig. 10(b) the ac currents in the primary and secondary

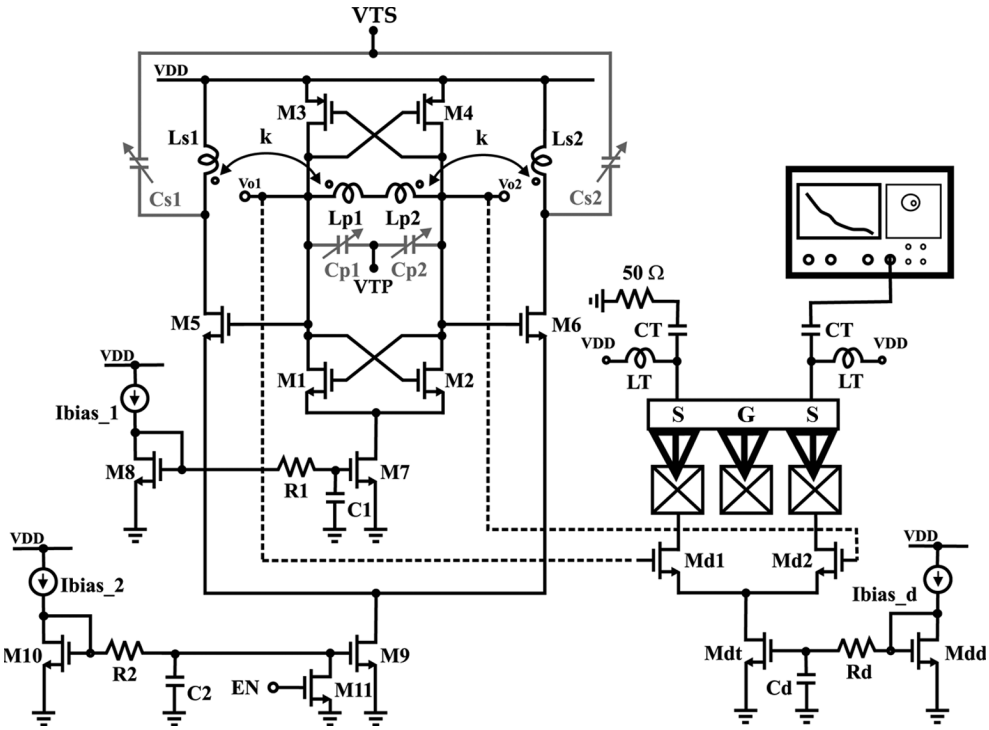

Fig. 11. Full schematic of the multi-band VCO including measurement setup.

windings are out of phase. Thus, when i_p charges energy to the tank, i_s discharge a portion of that energy depending on the transformer parameters. For this reason, the tank has less energy storage capability with respect to that of a stand-alone inductor. Quantitatively, it is the $(1-k)$ term in (4) that is responsible for the reduction in energy storage capability. However, it is the effect of coupling factor in the terms $(1-k)$ and $(1+k)$ that also provides multi-band operation through varying the effective inductance values. Techniques to compensate for the reduction in quality factor in high-band operation are discussed in Section III-C.

IV. VCO Design

Fig. 11 shows the schematic of the VCO utilizing the double-tuned, double-driven transformer as a resonator [32]. In the core of the oscillator, the negative resistance is realized by cross-coupled nMOS and pMOS pairs (M1–M4). The cross-coupled complementary topology is selected because of its reduced 1/f noise up-conversion performance [33]. The core resonator is formed of Cp1 and Cp2, and the primary inductors of the transformers Lp1 and Lp2. The primary inductance L1 is selected as 1.6 nH, while the secondary L2 is 2.8 nH. Accumulation mode varactors are used for fine tuning purposes. The primary varactors are implemented as 6×3 fingers ($W=5\ \mu\text{m}, L=1\ \mu\text{m}$), while the secondary varactor is formed by 6×7 fingers ($W=5\ \mu\text{m}, L=1\ \mu\text{m}$). The transformer has a Q of 12 at 2 GHz while Q is variable at high-band as a function of the driver stage's transconductance. The current source shown in Fig. 8 which drives the secondary port of the transformer is realized using a simple differential pair (M5–M6) loaded with the secondary windings of the transformers, Ls1 and Ls2. The band switching is controlled by enabling and disabling the differential pair, while the inverting nature of the common source amplifier provides the required phase difference between primary and secondary winding currents for multi-band operation. When the differential pair is disabled by turning off the tail current source transistor M9 via transistor M11, no driving current passes in the secondary port. Thus, the oscillator swings at low-band frequencies, acting as a single-band LC VCO which has a transformer type resonator. When the tail current is enabled and the secondary port is driven by the differential pair, the oscillator swings at high-band and the low-band oscillation is suppressed. The oscillator frequency in each band can be tuned by changing the control voltages VTP and VTS, which control the effective capacitance of the primary and secondary varactors (Cp1, Cp2) and (Cs1, Cs2). In the current mirrors, RC filters are employed to filter 1/f noise of the diode connected transistors. In the actual implementation, to prove the concept, each transformer is realized individually. However, they could also be realized as a differentially driven single transformer to save area further.

A. Design of Driver Stage

Although the driver transistors (M5 and M6) are not used as switches in the frequency generation loop, their parasitics may still contribute to the tuning range and phase noise. The buffer transistors are selected wide enough to drive the secondary winding; but the width is still limited so as not to load the tank considerably. The selected aspect ratio for the buffer transistors is $100\ \mu\text{m}/0.25\ \mu\text{m}$, which is much smaller than switched resonator examples ($960\ \mu\text{m}/0.18\ \mu\text{m}$ and $2000\ \mu\text{m}/0.18\ \mu\text{m}$ [11], [12]). Thus, it can be safely stated that the effect of the parasitic capacitance of the proposed method over the frequency tuning range is negligible with respect to that of switched inductor/capacitor technique. The potential resistive loss of the proposed technique may originate from the output resistance of the driver transistors. However, in the switched

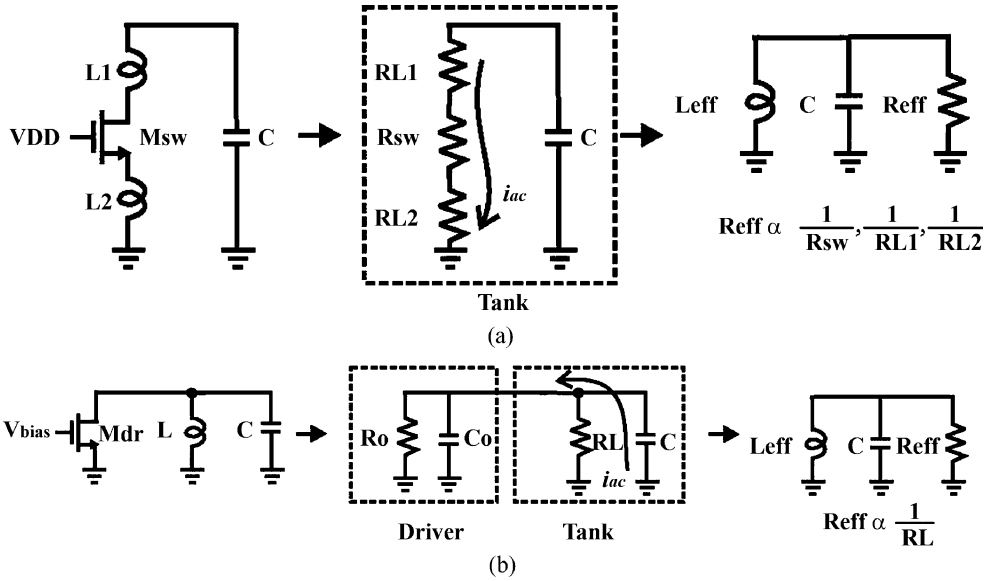

Fig. 12. Comparison of the loss contribution of the MOS transistors used in multi-band operation. (a) Switched inductor. (b) Driven inductor.

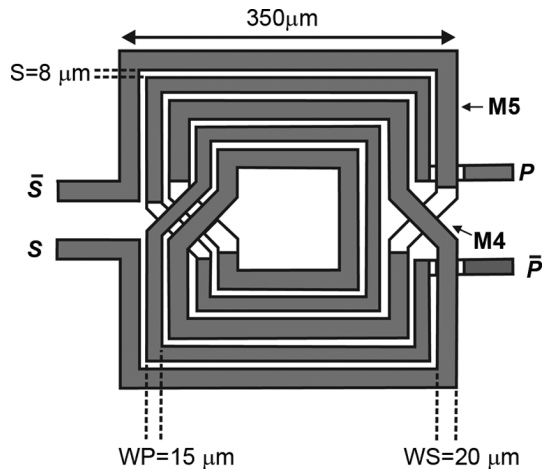

Fig. 13. Physical design of the transformer employed in the multi-band VCO tank.

inductor/capacitor tank shown in Fig. 12(a), the AC current that stores energy in the tank flows *through* the switch transistors that operate in triode region, thus the switch transistor contributes directly to the parallel equivalent loss resistance. For the driven inductor case in Fig. 12(b), the transistors operate in the saturation region exhibiting high output impedance. The tank is driven by a current source and the AC current completes its loop over the tank as shown in Fig. 12(b). Thus, the driver transistors do not cause substantial resistive loss.

B. Design of the Transformer

The transformer used in the resonator design is shown in Fig. 13. A square symmetric topology (Rabjohn balun) is selected for the resonator design. The top thick metal5 layer $(2\ \mu\text{m})$ in the used technology is employed for the transformer implementation and metal-4 is used for crossings. The primary winding width is $15\ \mu$m. The secondary winding width is selected as $20\ \mu$m in order to reduce the parasitic resistance of secondary winding. The transformer is simulated with Sonnet EM tool. For the transient simulations, a 10-segment distributed RLC-k equivalent circuit that covers DC-to-10 GHz range is created and its parameters are fitted to s-parameter simulation results of the EM tool. Thus, the effect of the virtual ac ground in the middle of the tank is avoided using a distributed equivalent model instead of a lumped model. In the design of the transformer, two issues have to be addressed: 1) achieving a low coupling coefficient and 2) reducing the sensitivity of the coupling coefficient to the physical design of the transformer, specifically spacing. For the low coupling coefficient, the spacing is varied from the design rules minimum spacing up to $20\ \mu$m. The gradient of coupling coefficient with line spacing saturates around $7 \sim 8\ \mu$m spacing, thus limiting the effect of process variation on the coupling coefficient. A minimum coupling coefficient of $0.6 \sim 0.65$ is obtained at a spacing of $8\ \mu$m, and any further increase in the line spacing would not reduce the coupling coefficient considerably. In fact, if the area and spacing are limited to practically reasonable values, this k value would be the lowest for this topology. An extensive research on the same topology [34] confirms our results. To obtain lower coupling coefficient $(0.4 \sim 0.5)$, other transformer topologies such as concentric spirals should be employed. This would ultimately lead to improved performance especially in the high frequency band.

C. Design Considerations

The power consumption of the VCO is limited by four main factors:

1) feature size of the selected process;
2) selected topology;
3) transformer coupling coefficient k;
4) top metal thickness.

Because the threshold voltage dictates the voltage headroom, the feature size of the selected topology has an important effect on the power consumption. Even for the same topology and the same tank, which primarily determines the drawn current for the

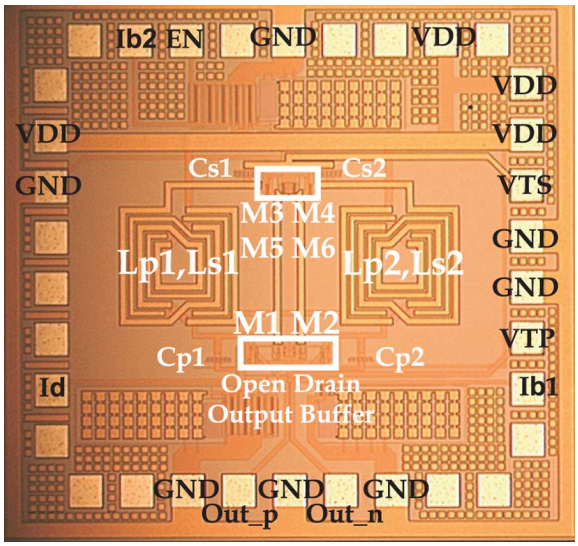

Fig. 14. Die photo of the multi-band VCO.

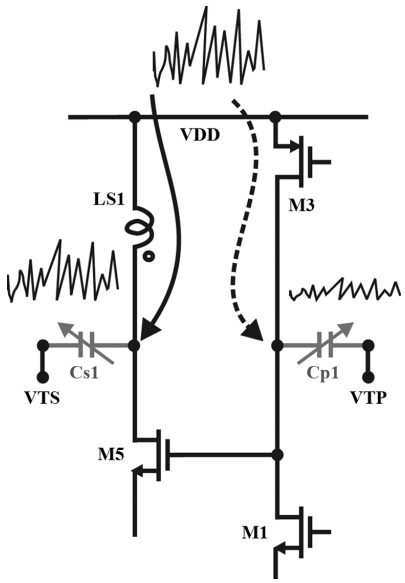

Fig. 15. Supply noise coupling paths in multi-band VCO.

same output power, the technology with the higher feature size leads to relatively higher power consumption. In the implementation discussed, the feature size (0.25 μm) is a bottleneck, when compared to lower feature sizes. A migration to 90 nm and below technologies will provide at least 30% drop in power consumption assuming the same topology.

The selected topology is another limitation over voltage headroom. Although the cross coupled complementary topology reduces the up-conversion of 1/f noise, it also requires more voltage headroom because of the cascode nMOS and pMOS transistors.

There is a strong relation between transformer coupling coefficient and parallel equivalent loss resistance of the tank at low-band and high-band. If k is selected higher than the required value, it is expected to have a very low parallel equivalent loss resistance at high-band resonance point that requires high current to get the same output power at the low-band [Fig. 9(c)]. Thus, once the required specifications are determined in terms of operation bands and phase noise, k should be selected taking into account the overall power consumption requirements.

The last issue that affects the overall power consumption is the metal thickness. The thickness may vary from 0.3 μm to 0.5 μm for the inter-level metals layer. However, some processes offer thicker top metals ranging from 2 μm to 4 μm. Also in some other examples, the stacked metals are connected throughout the inductor by vias to obtain a thicker metal effectively. In the current design, the top metal which has a thickness of 2 μm is used. However, thicker metal would definitely reduce the series resistance and thus power consumption.

V. Experimental Results

The multi-band CMOS LC VCO is implemented in a five-metal 0.25 μm TSMC CMOS technology. The micrograph of the fabricated VCO is shown in Fig. 14. The chip is mounted on a FR-4 board and measured in a screened-room. Agilent E5052A signal source analyzer is used for phase noise measurements. The measured single-ended output is taken from an open-drain buffer, supplied through off-chip bias-tees as shown in Fig. 11. The output driver is designed such that it can deliver an output power over 0 dBm to a 50-ohm load.

For the measurements in the high-frequency band, the supply noise affected the measurement. This is mainly due to the low resistance path between the secondary varactors and supply lines as shown in Fig. 15. At high-band, because of the relatively low resistance path between supply line and the points at which the varactors are connected to the tank, the supply noise can leak to tank. This modulates the effective control voltage over the secondary varactors, which translates into drifting in the center frequency. Because the pMOS transistors provide relatively higher attenuation, this problem is not the case for low-band operation.

This common-mode noise problem can be reduced by using differential tuning. Thus, the noise that occurs as a common-mode signal can be rejected. The supply voltage for the driver can be internally regulated as well.

The VCOs tuning characteristics is shown in Fig. 16(a) for low-band and high-band operation. The VCO has two separate tuning voltage control inputs. The tuning range is characterized by changing the control voltages at the primary port VTP, and secondary port VTS independently as defined in Table I. The VCO is tunable from 1.94 to 2.55 GHz at low-band and from 3.6 to 4.77 GHz at high-band. Fig. 16(b) shows the VCO gain as a function of control voltage. While the varactor connected to the secondary windings is directly connected to VDD, the primary varactors' gate is biased at a voltage less than VDD due to the voltage drop across the pMOS transistors. Thus, as can be seen from Fig. 16(b), the primary tuning varactor has its maximum gain around 1.4 V while secondary varactor has its highest gain around 2 V. Fig. 16(b) also shows that oscillation frequency is more sensitive to the value of secondary varactor capacitance.

To guarantee that while operating in one band, the second frequency band is totally suppressed, we measured the output spectrum of the oscillator at the borders of each band as in Fig. 17. Fig. 17(a) and (b) shows the output oscillation at the

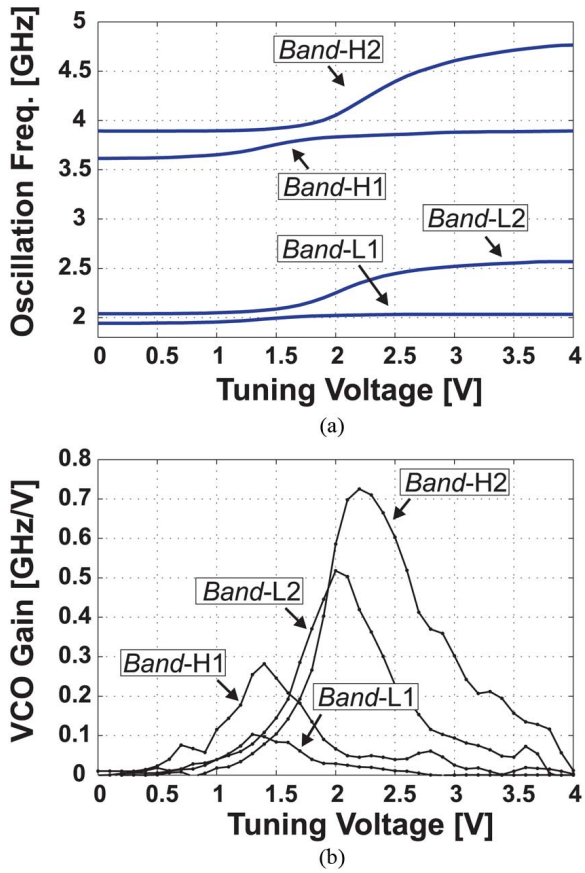

Fig. 16. (a) Measured tuning range of the VCO for the low and high bands. (b) VCO gain ($K_{\rm VCO}$) versus tuning voltage.

TABLE I
SETTINGS OF PRIMARY VARACTORS, SECONDARY VARACTORS, AND SECONDARY DRIVING STAGE FOR DIFFERENT VCO TUNING OPTIONS

	VTP	VTS	Resonator Configuration
Band-L1	Variable 0-4 V	Fixed 0V	Single Driven
Band-L2	Fixed 4V	Variable 0-4 V	Single Driven
Band-H1	Variable 0-4 V	Fixed 0V	Double Driven
Band-H2	Fixed 4V	Variable 0-4 V	Double Driven

borders of the low frequency band 1.94 GHz and 2.55 GHz with the presence of the harmonic tones. Note that the existence of second and fourth harmonic tones is due to single-ended measurements. The second harmonic amplitude is 34 dB below the fundamental amplitude for the 1.94 GHz and 30 dB below the fundamental amplitude for 2.54 GHz. Fig. 17(c) shows the lower end of the high frequency band at 3.6 GHz with a second harmonic at 7.2 GHz with amplitude of 30.5 dB below the fundamental. Fig. 17(d) shows the higher end of the high frequency band at 4.77 GHz and amplitude of -9 dBm, and with a second harmonic almost 38 dB below the fundamental. It is clear from Fig. 17 that there are no low-band/high-band concurrent oscillations, and that the current-driven band switching mechanism completely eliminates one band when the other band is active.

The phase noise of the oscillator was measured over and at the borders of the operating bands for various cases. Fig. 18 shows three example plots for low-band and high-band. While the characteristic of the phase noise plot is as expected for low-band measurements at 1.94 GHz and 2.55 GHz, the measurement at 3.6 GHz exemplifies the supply noise effect at closer frequency offsets at high-band. To show an example of the variation characteristic of phase noise over the tuning ranges, the phase noise is measured at 1 MHz from the low-band and high-band carriers as shown in Fig. 19. For the low-band, the core current (I1) is selected arbitrarily at 1.5 mA while for the high-band the core current is 1.8 mA and driver current (I2) is 6 mA. The overall performance of the VCO is summarized in Table II.

Figs. 20 and 21 show the different bias scenarios for optimum phase noise performance at low-band and high-band. For low-band, the core bias current (I1) is varied at 1.94 GHz and under 1.8 V and 1.5 V supply voltage, which is the minimum supply voltage for the circuit to oscillate. For both supply voltages, the phase noise improvement saturates around 3.4 mA as shown in Fig. 20. For high-band, both currents I1, and I2 affect the phase noise performance. As seen in Fig. 21, different combinations of I1 and I2 lead to the same phase noise. For example, for the case of phase noise at 1 MHz offset from 3.6 GHz carrier, and if we consider points A and B, the same phase noise performance (~ -122.0 dBc/Hz) is obtained at $1.8+5.5$ mA and $1.2+9.5$ mA. Thus, the selection of (I1, I2) is critical in realizing optimum phase noise performance without dissipating unnecessary power.

The following power-frequency-tuning normalized (PFTN) figure of merit (FOM) that includes the tuning range [35] is used to compare the performance of the proposed VCO to published results in similar technology nodes:

$$\mathrm{PFTN} = 10\log\left[\frac{kT}{P_{\rm sup}}\cdot\left(\frac{f_{\rm tune}}{f_{\rm off}}\right)^2\right] - L\{f_{\rm off}\} \qquad (19)$$

where $P_{\rm sup}$ is the power dissipation, $f_{\rm tune}$ is the tuning range and $f_{\rm off}$ is the frequency offset from the carrier frequency at which phase noise is measured [35]. Note that the figure of merit expression does not explicitly take into account the technology effect (feature size, speed, etc.). However, having two oscillators in two different technologies, even with the same drawn current from the supply, one would have lower power consumption than the other due to the effect of lower threshold voltage. Therefore, for a fair comparison only the examples that are implemented in comparable technologies are included in Fig. 22. Table III summarizes the performance parameters for the same examples. The figure shows that the proposed approach has the highest FOM compared to published multi-band frequency generation circuits in similar technology nodes, while providing

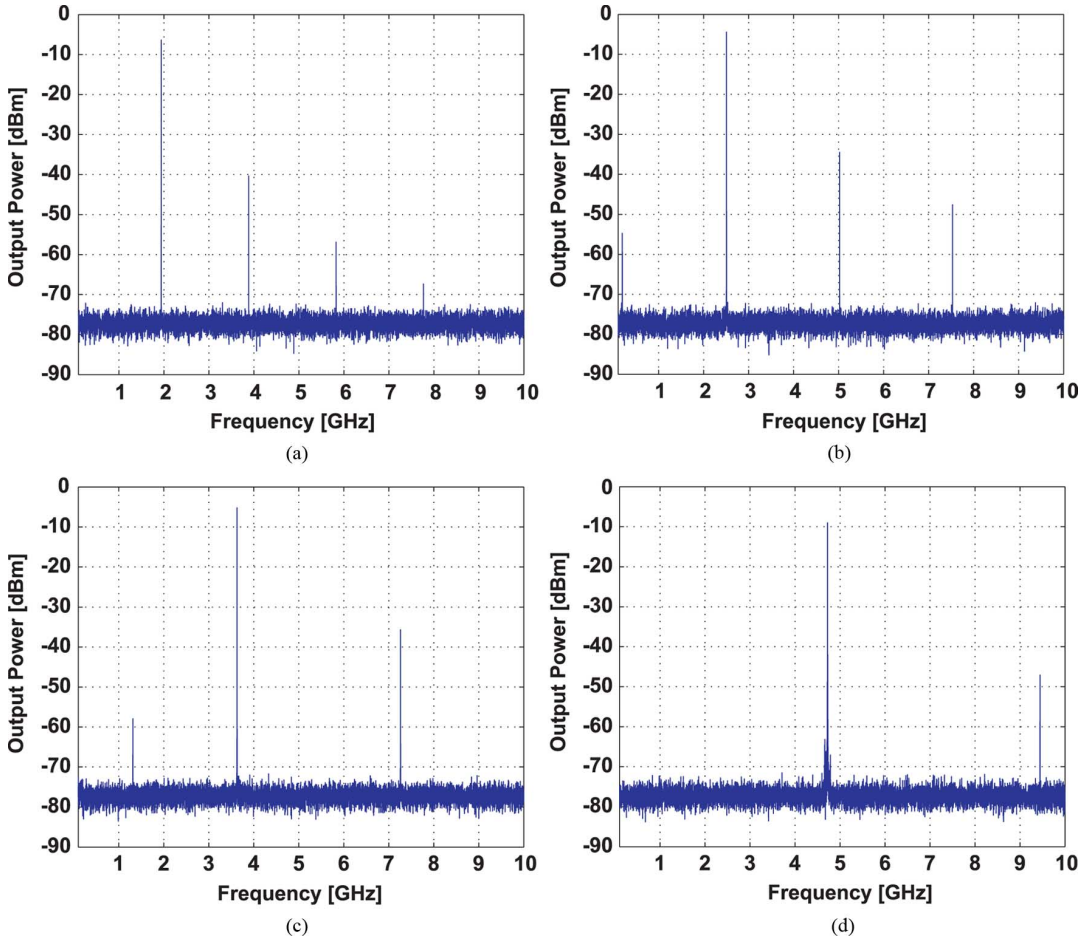

Fig. 17. Output spectrum of the VCO at the borders of its operation bands. (a) 1.94 GHz. (b) 2.54 GHz. (c) 3.64 GHz. (d) 4.76 GHz.

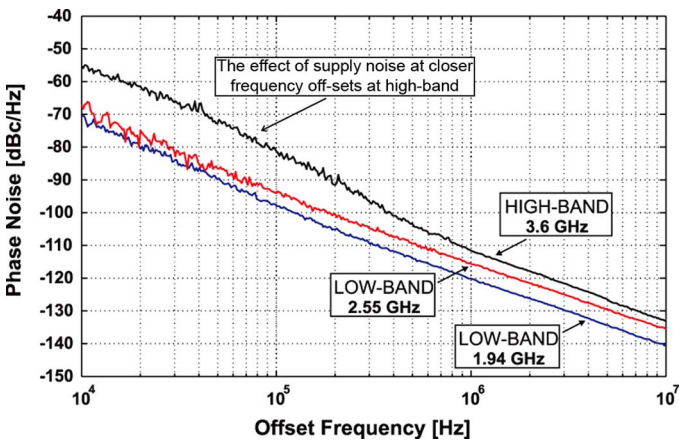

Fig. 18. Phase noise performance of the VCO at 1.94 GHz, 2.55 GHz, and 3.6 GHz.

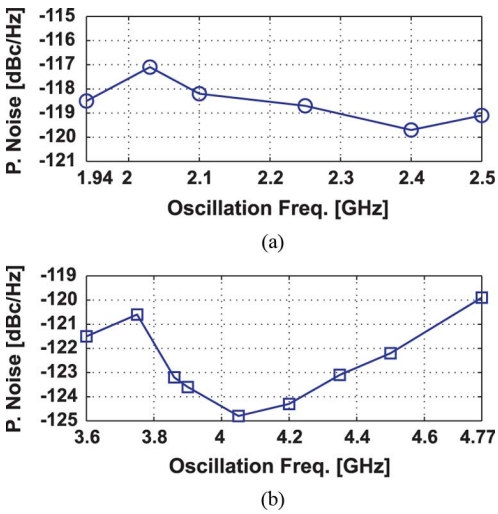

Fig. 19. Phase noise at 1 MHz offset from the carrier as function of oscillation frequency. (a) Low band. (b) High band.

wide tuning range characteristics. The power consumption can be further reduced in the high-band by using other transformer topologies with lower coupling coefficient.

VI. Conclusion

The use of double-tuned, double-driven transformers is proposed for the realization of dual-band oscillators. Band switching is provided by injecting current in the secondary port of the transformer load thus mitigating the effects on phase noise and tuning range resulting from connecting switches directly to the oscillator tank. The conditions required to start oscillations are derived for single-driven and double-driven, double-tuned transformers, explaining the nature of the band-

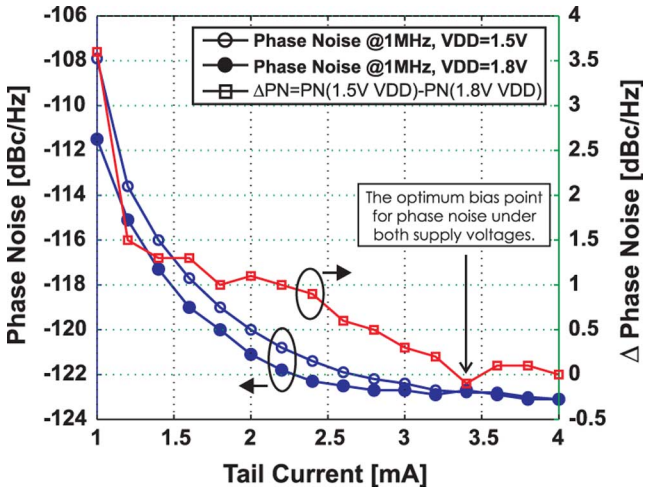

Fig. 20. Phase noise measurements at 1 MHz offset from 1.94 GHz carrier as a function of core bias current (I1) and supply voltage.

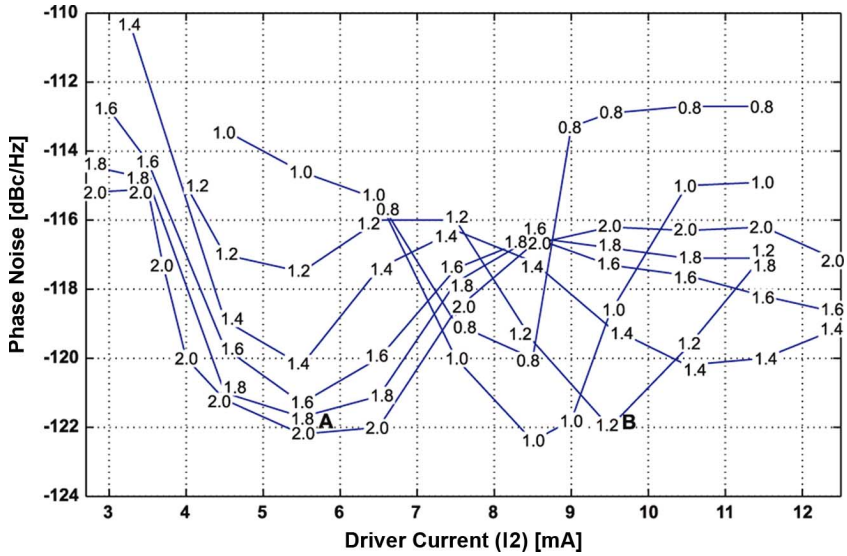

Fig. 21. Phase noise at 1 MHz offset from 3.6 GHz carrier (lower boundary of the high resonance point) as a function of driver and core currents I2 and I1, respectively.

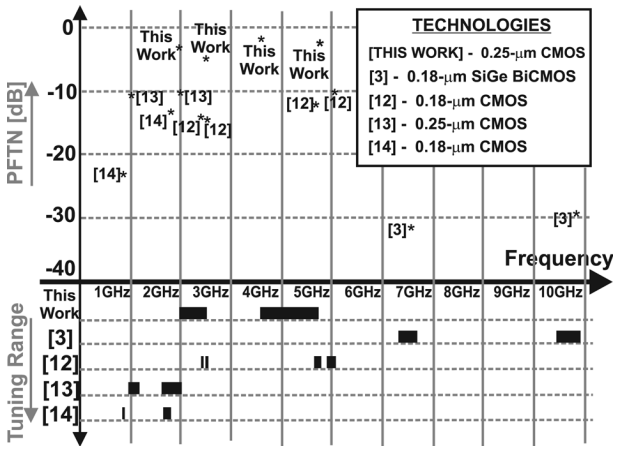

Fig. 22. FOM and tuning range comparison of published results in similar technology nodes and the proposed multi-band VCO.

TABLE II
VCO PERFORMANCE SUMMARY

	Low Band		High Band	
VDD (V)	1.8		1.8	
Measurement Frequency (GHz)	1.94	2.55	3.6	4.77
I_{VDD} (mA)	1.8	1	2+5.5	1.6+8.5
Phase Noise (dBc/Hz) at 1MHz	-120	-116	-122.2	-122.8
Tuning Voltage (V)	0-4		0-4	
Tuning Range (MHz)	610		1170	

switching mechanism. The relation between the coupling factor, frequency band separation, and quality factor at the two frequency bands is discussed. The proposed multi-band voltage controlled oscillator, implemented in 0.25 μm CMOS technology, is capable of tuning over 1.94 to 2.55 GHz and 3.6 to 4.77 GHz and achieves one of the highest reported FOM

TABLE III
COMPARISON OF PUBLISHED MULTI-BAND FREQUENCY SOURCES IN SIMILAR TECHNOLOGY NODES

Reference	Technology	Tuning Range [GHz]	Phase Noise [dBc/Hz] @ carrier [GHz]	Power [mW]	FOM [dB]
[3]	0.18-μm SiGe BiCMOS	6.3-6.6 9.45-9.9	@1MHz Offset -106 @ 6 GHz Mode -104 @ 9 GHz Mode	19.44 19.44	-31.1 -29.6
[12]	0.18-μm CMOS	2.40-2.44 2.47-2.52 4.65-4.80 4.92-5.12	@1MHz Offset -134 @ 2.42 -132 @ 2.51 -126 @ 4.72 -125 @ 5.01	4.6 4.6 6 6	-14.4 -14.4 -12.1 -10.6
[13]	0.25-μm CMOS	0.978-1.160 1.600-2.010	@3MHz Offset -138 @ 1 -132 @ 2	11.25 13.50	-10.6 -10.4
[14]	0.18-μm CMOS	0.823-0.867 1.640-1.814	@0.6MHz Offset -125 @ 0.865 -123 @ 1.812	16	-23.5 -13.6
This Work	0.25-μm CMOS	1.94-2.55 3.6-4.77	@1MHz Offset -120 @ 1.94 -116 @ 2.5 -122 @ 3.6 122 @ 4.77	3.24 1.8 13.5 18.18	-3.24 -4.6 -1.5 -2.2

compared to published oscillators in similar technology nodes, while providing multi-band operation, wide tuning range characteristics, with low power consumption.

ACKNOWLEDGMENT

The authors acknowledge Fred Schindler, Charles Wang, Brian McNamara, Paul Martinyuk, Ginny Lacquio, and Wilfer Fernandez from RF Micro Devices for their help in measurements.

REFERENCES

[1] F. Agnelli *et al.*, "System analysis and design of a reconfigurable RF front-end," *IEEE Circuits Devices Mag.*, pp. 38–59, First Quarter, 2006.

[2] R. Bagheri *et al.*, "An 800-MHz–6-GHz software-defined wireless receiver in 90-nm CMOS," *IEEE J. Solid-State Circuits*, vol. 41, no. 12, pp. 2860–2875, Dec. 2006.

[3] H. Shin, Z. Xu, and M. F. Chang, "A1.8-V6/9-GHz reconfigurable dual-band quadrature LC VCO in SiGe BiCMOS technology," *IEEE J. Solid-State Circuits*, vol. 38, no. 6, pp. 1028–1032, Jun. 2003.

[4] Liang *et al.*, "A 14-band frequency synthesizer for MB-OFDM UWB applications," in *IEEE Int. Solid-State Circuits Conf. Dig. Tech. Papers*, Feb. 2006, pp. 428–437.

[5] Leenaerts *et al.*, "A SiGe BiCMOS 1 ns fast-hopping frequency synthesizer for ultra wide band radio," in *IEEE Int. Solid-State Circuits Conf. Dig. Tech. Papers*, Feb. 2005, vol. 1, pp. 202–593.

[6] A. D. Berny, A. M. Niknejad, and R. G. Meyer, "A 1.8 GHz LC VCO with 1.3 GHz tuning range and digital amplitude calibration," *IEEE J. Solid-State Circuits*, vol. 40, no. 4, pp. 909–917, Apr. 2005.

[7] J. Kucera, "Wideband BiCMOS VCO for GSM/UMTS direct conversion receivers," in *IEEE Int. Solid-State Circuits Conf. Dig. Tech. Papers*, Feb. 2001, pp. 374–375.

[8] K. Manetakis, D. Jessie, and C. Narathong, "A wideband CMOS VCO for zero-IF GSM-CDMA single-chip transceiver," in *Proc. European Solid-State Conf. (ESSCIRC)*, Sep. 2004, pp. 139–142.

[9] K. Kwok and J. Long, "A 23-to-29 GHz transconductor-tuned VCO MMIC in 0.13 μm CMOS," *IEEE J. Solid-State Circuits*, vol. 42, no. 12, pp. 2878–3997, Dec. 2007.

[10] J. Cho, H. Lee, K. Nah, and B. Park, "A 2-GHz wideband low phase noise voltage-controlled oscillator with on-chip LC tank," in *Proc. IEEE Custom Integrated Circuits Conf. (CICC)*, 2003, pp. 559–562.

[11] Z. Li and K. K. O, "A 900-MHz 1.5-V CMOS voltage-controlled oscillator using switched resonators with a wide tuning range," *IEEE Microwave Wireless Compon. Lett.*, vol. 13, no. 4, pp. 137–139, Apr. 2003.

[12] Z. Li and K. K. O, "A low-phase-noise and low-power multi-band CMOS voltage-controlled oscillator," *IEEE J. Solid-State Circuits*, vol. 40, no. 6, pp. 1296–1302, Jun. 2005.

[13] M. Tiebout, "A CMOS fully integrated 1 GHz and 2 GHz dual-band VCO with a voltage controlled inductor," in *Proc. Eur. Solid-State Circuits Conf. (ESSCIRC)*, Florence, Italy, Sep. 2002, pp. 799–802.

[14] S.-M. Yim and K. K. O, "Switched resonators and their applications in a dual-band monolithic CMOS LC-tuned VCO," *IEEE Trans. Microw. Theory Tech.*, vol. 54, no. 1, pp. 74–81, Jan. 2006.

[15] G. Cumai, M. Repossi, G. Albasini, A. Mazzzanti, and F. Svelto, "A magnetically tuned quadrature oscillator," *IEEE J. Solid-State Circuits*, vol. 42, pp. 2870–2877, Dec. 2007.

[16] L. H. Lue *et al.*, "A wide tuning-range CMOS VCO with a differential tunable active inductor," *IEEE Trans. Microw. Theory Tech.*, vol. 54, no. 9, pp. 3462–3468, Sep. 2006.

[17] A. Bevilacqua *et al.*, "Transformer-based dual-mode voltage-controlled oscillators," *IEEE Trans. Circuits Syst. II: Express Briefs*, vol. 54, no. 4, pp. 293–297, Apr. 2007.

[18] A. Goel *et al.*, "Frequency switching in dual-resonance oscillators," *IEEE J. Solid-State Circuits*, vol. 42, no. 3, pp. 571–582, Mar. 2007.

[19] Z. Safarian *et al.*, "A 1.3–6 GHz triple-mode CMOS VCO using coupled inductors," in *Proc. IEEE Custom Integrated Circuits Conf. (CICC)*, 2008, pp. 69–72.

[20] D. Hauspie *et al.*, "Wideband VCO with simultaneous switching of frequency band, active core, and varactor size," *IEEE J. Solid-State Circuits*, vol. 42, no. 7, pp. 1472–1480, Jul. 2007.

[21] P. Andreani *et al.*, "A 1.8-GHz monolithic CMOS VCO tuned by an inductive varactor," in *IEEE Int. Symp. Circuits Syst. (ISCAS)*, May 2001, vol. 4, pp. 714–717.

[22] F. Herzel, H. Erzgraber, and N. Ilkov, "A new approach to fully integrated CMOS LC-oscillators with very large tuning range," in *Proc. IEEE Custom Integrated Circuits Conf. (CICC)*, May 2000, pp. 573–576.

[23] D. Nguyen, "Exploit leakage inductance in VCO design," *Microwaves & RF*, pp. 59–60, 62, 66-67, 187, Nov. 1999.

[24] M. Demirkan, S. P. Bruss, and R. R. Spencer, "11.8 GHz CMOS VCO with 62% tuning range using switched coupled inductors," in *2007 IEEE Radio Frequency Integrated Circuits (RFIC) Symp.*, Jun. 2007, pp. 401–404.

[25] M. T. Reiha and J. R. Long, "A 1.2 V reactive-feedback 3.1–10.6 GHz low-noise amplifier in 0.13 μm CMOS," *IEEE J. Solid-State Circuits*, vol. 42, no. 5, pp. 1023–1033, May 2007.

[26] M. Straayer, J. Cabanillas, and G. M. Rebeiz, "A low-noise transformer-based 1.7 GHz CMOS VCO," in *2002 IEEE Int. Solid-State Circuits Conf. (ISSCC) Dig. Tech. Papers*, Feb. 2002, vol. 1, pp. 286–287.

[27] H. L. Krauss, C. W. Bostian, and F. H. Raab, *Solid State Radio Engineering*. New York: Wiley, 1980.

[28] B. Çatlı and M. Hella, "Dual-band ultra-wide tuning range CMOS voltage-controlled oscillator," *Electron. Lett.*, vol. 42, no. 21, pp. 1215–1216, Oct. 2006.

[29] P. Andreani and J. R. Long, "Misconception regarding use of transformer resonators in monolithic oscillators," *Electron. Lett.*, vol. 42, no. 7, pp. 387–388, Mar. 2006.

[30] H. Hashemi, "Integrated concurrent multi-band radios and multiple antenna systems," Ph.D. dissertation, California Inst. Technol , Pasadena, CA, 2003.

[31] H. Krishnaswamy and H. Hashemi, "Inductor-and transformer-based integrated RF oscillators: A comparative study," in *Proc. IEEE Custom Integrated Circuits Conf. (CICC)*, Sep. 2006, pp. 381–384.

[32] B. Çatlı and M. Hella, "A dual-band, wide tuning range CMOS voltage controlled oscillator for multi-band radio," in *IEEE Radio Frequency Integrated Circuits (RFIC) Symp. Dig.*, Jun. 2007, pp. 595–598.

[33] A. Hajimiri and T. H. Lee, "Design issues in CMOS differential LC oscillators," *IEEE J. Solid-State Circuits*, vol. 34, no. 5, pp. 717–724, May 1999.

[34] G. G. Rabjohn, "Monolithic microwave transformers," M.Eng. thesis, Carleton Univ., Ottawa, ON, Canada, 1991.

[35] D. Ham and A. Hajimiri, "Concepts and methods in optimization of integrated LC VCOs," *IEEE J. Solid-State Circuits*, vol. 36, no. 6, pp. 896–909, Jun. 2001.

Burak Çatlı (S'96) received the B.S. and M.S. degrees in electronic engineering from Istanbul Technical University, Istanbul, Turkey, in 1998 and 2001, respectively. He is currently working toward the Ph.D. degree in the Electrical, Computer, and Systems Engineering Department, Rensselaer Polytechnic Institute, Troy, NY.

He was a graduate student and research assistant in the Electronic and Communication Engineering Department, Istanbul Technical University, between 1998 and 2005. From 1998 to 2005, he was a design engineer with the ETA-IC Design Center, Istanbul, Turkey, developing RF front-end blocks and high-speed high-resolution data converter systems for industrial and military applications. During summers of 2006 and 2007, he was with RF Micro Devices, Boston, MA, and during summer of 2008, he was with Qualcomm Inc., Santa Clara, CA . His research interests are in the area of analog and mm-wave circuit design for integrated communication systems.

Mr. Catlı was awarded at the 2007 Analog Devices Mixed Signal Design Contest for the best industrial grade design and was the recipient of 2007 Veera and Arjun Saxena Fellowship in Microelectronics.

Mona Mostafa Hella (S'96–M'01) received the B.Sc. and Master degrees with Honors from Ain-Shams University, Cairo, Egypt, in 1993 and 1996, and the Ph.D. degree from the Ohio State University, Columbus, OH, in 2001, all in electrical engineering.

From 1993 to 1997, she was a teaching and research assistant at Ain Shams University. From 1997 to 2001, she was a research assistant at the Ohio State University. She was with the Helsinki University of Technology, Espoo, Finland, as a visiting scholar in the summer of 1998, and with the analog group at Intel, Chandler, AZ, in summer of 1999. She was a Senior Designer at Spirea AB, Stockholm, Sweden, working on CMOS power amplifiers during 2000–2001. From 2001 to 2003, she was a Senior Designer at RFMD Inc, Billerica, MA, working on optical communication systems, as well as silicon-based wireless systems. She joined the Electrical, Computer and Systems Engineering Department, Rensselaer Polytechnic Institute, Troy, NY, as an Assistant Professor in 2004. Her research interests include mixed-signal and RFIC design for wireless and wire-line applications.